

On-Line Palmprint Identification

David Zhang, *Senior Member, IEEE*,
Wai-Kin Kong, *Member, IEEE*,
Jane You, *Member, IEEE* and Michael Wong

Biometrics Research Centre
Department of Computing
The Hong Kong Polytechnic University
Kowloon, Hong Kong
csdzhang{cswkkong, csyjia, csmkwong}@comp.polyu.edu.hk

Corresponding author:

Prof. David Zhang
Biometrics Research Centre
Department of Computing
The Hong Kong Polytechnic University
Hung Hom, Kowloon, Hong Kong
Phone: (852) 2766-7271
Fax: (852) 2774-0842
E-mail: csdzhang@comp.polyu.edu.hk

Abstract — Biometrics based personal identification is regarded as an effective method for automatically recognizing, with a high confidence, a person's identity. This paper presents a new biometric approach to on-line personal identification using palmprint technology. In contrast to the existing methods, our on-line palmprint identification system employs low-resolution palmprint images to achieve effective personal identification. The system consists of two parts: a novel device for on-line palmprint image acquisition, and an efficient algorithm for fast palmprint recognition. A robust image coordinate system is defined to facilitate image alignment for feature extraction. In addition, a 2-D Gabor phase encoding scheme is proposed for palmprint feature extraction and representation. The experimental results demonstrate the feasibility of the proposed system.

Index Terms — Biometrics, on-line palmprint identification, texture analysis, low-resolution image.

1 INTRODUCTION

The rapid growth in the use of *e-commerce* applications requires reliable and automatic personal identification for effective security control. Traditional, automatic, personal identification can be divided into two categories: token-based, such as a physical key, an ID card and a passport, and knowledge-based, such as a password. However, these approaches have some limitations. In the token-based approach, the “token” can be easily stolen or lost. In the knowledge-based approach, to some extent, the “knowledge” can be guessed or forgotten. Thus, biometric personal identification is emerging as a powerful means for automatically recognizing a person's identity. The biometric computing based approach is concerned with identifying a person by his/her physiological characteristics, such as iris pattern, retina, palmprint, fingerprint and face, or using some aspect of his/her behavior, such

as voice, signature and gesture [1-2]. Fingerprint-based personal identification has drawn considerable attention over the last 25 years [17]. However, workers and elderly may not provide clear fingerprint because of their problematic skins and physical work. Recently, voice, face and iris-based verifications have been studied extensively [1-2,12-16]. As a result, many biometric systems for commercial applications have been successfully developed. Nevertheless, limited work has been reported on palmprint identification and verification, despite the importance of palmprint features.

There are many unique features in a palmprint image that can be used for personal identification. Principal lines, wrinkles, ridges, minutiae points, singular points and texture are regarded as useful features for palmprint representation [6]. Various features can be extracted at different image resolutions. For features such as minutiae points, ridges and singular points, a high-resolution image, with at least 400 dpi (dots per inch), is required for feature extraction [7]. However, features like principal lines and wrinkles, which are defined in Fig. 1, can be obtained from a low-resolution palmprint image with less than 100 dpi [3,6]. In general, high-resolution images are essential for some applications such as law enforcement, where ridges, singular points and minutiae points are extracted and matched in latent prints for identification and verification. Some companies, including NEC and PRINTRAK, have developed automatic palmprint identification and verification systems for law enforcement applications [8,20]. For civil and commercial applications, low-resolution palmprint images are more suitable than high-resolution images because of their smaller file sizes, which results in shorter computation times during preprocessing and feature extraction. Therefore, they are useful for many real-time palmprint applications.

Automatic palmprint identification systems can be classified into two categories: *on-line* and *off-line*. An on-line system captures palmprint images using a palmprint capture sensor that is directly connected to a computer for real-time processing. An off-line palmprint

identification system usually processes previously captured palmprint images, which are often obtained from inked palmprints that were digitized by a digital scanner. In the past few years, some researchers have worked on off-line palmprint images and have obtained useful results [3-7,9]. Recently, several researchers have started to work on on-line palmprint images that are captured by CCD (charge-coupled device) cameras or digital scanners [18-19]. In contrast to the existing on-line approaches, we develop an on-line palmprint identification system, for civil and commercial applications, that uses low-resolution images.

There are three key issues to be considered in developing an on-line palmprint identification system:

- 1) Palmprint Acquisition: How do we obtain a good quality palmprint image in a short time interval, such as 1 second? What kind of device is suitable for data acquisition?
- 2) Palmprint Feature Representation: Which types of palmprint features are suitable for identification? How to represent different palmprint features?
- 3) Palmprint Identification: How do we search for a queried palmprint in a given database and obtain a response within a limited time?

So far, several companies have developed special scanners to capture high-resolution palmprint images [8,20]. These devices can extract many detailed features, including minutiae points and singular points, for special applications. Although these platform scanners can meet the requirements of on-line systems, they are difficult to use in real-time applications because a few seconds are needed to scan a palm. To achieve on-line palmprint identification in real-time, a special device is required for fast palmprint sampling. Previously our research team has successfully developed a CCD camera based on a special device for on-line palmprint acquisition. A brief description of this special device is presented in Section 2.1.

Palmprint feature representation depends on image resolution. In high-resolution palmprint images (> 400 dpi), many features that are similar to singular points and minutiae points in a fingerprint can be obtained; however, these features cannot be observed in low-resolution images (< 100 dpi). Nevertheless, we can extract principal lines and wrinkles from low-resolution images. In fact, line features play an important role in palmprint identification [3-4]. Unfortunately, it is difficult to obtain a high recognition rate using only principal lines because of their similarity among different people. It is noted that texture representation for coarse-level palmprint classification provides an effective approach [5]. In this paper, we explore the use of texture to represent low-resolution palmprint images for on-line personal identification.

The rest of this paper is organized as follows. Section 2 gives a brief description of our low-resolution based, on-line palmprint identification system. A palmprint coding scheme and palmprint matching using hamming distance are detailed in Section 3. Section 4 reports our experimental results for both identification and verification. Finally, the conclusion and future work are presented in Section 5.

2 SYSTEM DESCRIPTION

In this paper, we utilize palmprint images with 75 dpi resolution to develop a real-time palmprint identification system that consists of two parts: a novel device for on-line palmprint image acquisition, and an effective algorithm for fast palmprint recognition.

2.1 On-line Palmprint Image Acquisition

Our palmprint capture device includes ring source, CCD camera, lens, frame grabber and A/D (analogue-to-digital) converter. To obtain a stable palmprint image, a case and a cover are used to form a semi-closed environment, and the ring source provides uniform lighting

conditions during palmprint image capturing. Also, six pegs on the platform serve as control points for the placement of the user's hands. The A/D converter directly transmits the images captured by the CCD camera to a computer. Fig. 2 shows a schematic diagram of our on-line palmprint capture device. Palmprint images can be obtained in two different sizes, 384×284 and 768×568.

2.2 Coordinate System: Preprocessing

It is important to define a coordinate system that is used to align different palmprint images for matching. To extract the central part of a palmprint, for reliable feature measurements, we use the gaps between the fingers as reference points to determine a coordinate system. The five major steps (see Fig. 3) in processing the image are:

Step 1: Apply a lowpass filter, $L(u, v)$, such as Gaussian smoothing, to the original image, $O(x, y)$. A threshold, T_p , is used to convert the convolved image to a binary image, $B(x, y)$, as shown in Fig. 3(b).

Step 2: Obtain the boundaries of the gaps, (F_{ix_j}, F_{iy_j}) ($i=1, 2$), between the fingers using a boundary tracking algorithm (see Fig. 3(c)). The boundary of the gap between the ring and middle fingers is not extracted since it is not useful for the following processing.

Step 3: Compute the tangent of the two gaps. Let (x_1, y_1) and (x_2, y_2) be any points on (F_{1x_j}, F_{1y_j}) and (F_{2x_j}, F_{2y_j}) , respectively. If the line $(y=mx+c)$ passing through these two points satisfies the inequality, $F_{iy_j} = mF_{ix_j} + c$, for all i and j (see Fig. 3(d)), then the line $(y = mx + c)$ is considered to be the tangent of the two gaps.

Step 4: Line up (x_1, y_1) and (x_2, y_2) to get the Y-axis of the palmprint coordinate system, and use a line passing through the midpoint of these two points, which is perpendicular to the Y-axis, to determine the origin of the coordinate system (see Fig. 3(d)).

Step 5: Extract a sub-image of a fixed size based on the coordinate system. The sub-image is located at a certain area of the palmprint image for feature extraction (see Figs. 3(e)-(f)).

3 PALMPRINT REPRESENTATION AND IDENTIFICATION

3.1 Feature Extraction and Coding

As mentioned before, a palmprint can be represented by some line features from a low-resolution image. Algorithms such as the stack filter [9] are able to extract the principal lines. However, these principal lines are not sufficient to represent the uniqueness of each individual's palmprint because different people may have similar principal lines in their palmprints. Fig. 4 demonstrates this problem by showing nine different palmprint samples that have similar principal lines. In addition, some palmprint images do not have clear wrinkles (see Fig. 5). As a result, we try to extract texture features from low-resolution palmprint images, and we propose a 2-D Gabor phase coding scheme for palmprint representation, which has been used for iris recognition [12].

The circular Gabor filter is an effective tool for texture analysis [12], and has the following general form,

$$G(x, y, \mathbf{q}, u, \mathbf{s}) = \frac{1}{2\pi\mathbf{s}^2} \exp\left[-\frac{x^2 + y^2}{2\mathbf{s}^2}\right] \exp\{2\pi i(ux\cos\mathbf{q} + uys\sin\mathbf{q})\}, \quad (1)$$

where $i = \sqrt{-1}$, u is the frequency of the sinusoidal wave, \mathbf{q} controls the orientation of the function, and \mathbf{s} is the standard deviation of the Gaussian envelope. To make it more robust against brightness, a discrete Gabor filter, $G[x, y, \mathbf{q}, u, \mathbf{s}]$, is turned to zero DC (direct current) with the application of the following formula:

$$\tilde{G}[x, y, \mathbf{q}, u, \mathbf{s}] = G[x, y, \mathbf{q}, u, \mathbf{s}] - \frac{\sum_{i=-n}^n \sum_{j=-n}^n G[i, j, \mathbf{q}, u, \mathbf{s}]}{(2n+1)^2}, \quad (2)$$

where $(2n+1)^2$ is the size of the filter. In fact, the imaginary part of the Gabor filter automatically has zero DC because of odd symmetry. The adjusted Gabor filter is used to filter the preprocessed images.

It should be pointed out that the success of 2-D Gabor phase coding depends on the selection of Gabor filter parameters, \mathbf{q} , \mathbf{s} , and u . In our system, we applied a tuning process to optimize the selection of these three parameters. As a result, one Gabor filter with optimized parameters, $\mathbf{q} = \pi/4$, $u = 0.0916$ and $\mathbf{s} = 5.6179$, is exploited to generate a feature vector with 2,048 dimensions. In addition, we also include an automatic *thresholding* procedure to handle the misplacement of the palm during data sampling. In some cases, a user does not place his/her hand correctly and some *non-palmprint pixels* will be included in the preprocessed images. A typical example is shown in Fig. 6, which shows the incorrect placement of a user's palm and the corresponding preprocessed palmprint image containing a redundant black region. To remove such redundant information from the image, we generate a mask to identify the location of the non-palmprint pixels. Based on the semi-closed environment of the scanning device, the non-palmprint pixels are mainly caused by the black boundaries of the platform. Thus, we can easily use a threshold to segment these non-palmprint pixels. Fig. 7 depicts the preprocessed images, showing the texture features obtained after 2-D Gabor filtering and the corresponding masks.

3.2 Palmprint Matching

Given two data sets, a matching algorithm determines the degree of similarity between them. To describe the matching process clearly, we use a feature vector to represent image data that consists of two feature matrices, real and imaginary. A normalized Hamming distance used in

[12] is adopted to determine the similarity measurement for palmprint matching. Let P and Q be two palmprint feature vectors. The normalized hamming distance can be described as,

$$D_o = \frac{\sum_{i=1}^N \sum_{j=1}^N P_M(i, j) \cap Q_M(i, j) \cap (P_R(i, j) \otimes Q_R(i, j) + P_I(i, j) \cap Q_M(i, j) \cap (P_I(i, j) \otimes Q_I(i, j)))}{2 \sum_{i=1}^N \sum_{j=1}^N P_M(i, j) \cap Q_M(i, j)}, \quad (3)$$

where $P_R(Q_R)$, $P_I(Q_I)$ and $P_M(Q_M)$ are the real part, the imaginary part and the mask of $P(Q)$, respectively. The result of the Boolean operator (\otimes) is equal to zero, if and only if the two bits, $P_{R(I)}(i, j)$, are equal to $Q_{R(I)}(i, j)$; the symbol \cap represents the AND operator, and the size of the feature matrixes is $N \times N$. It is noted that D_o is between 1 and 0. For the best matching, the hamming distance should be zero. Because of imperfect preprocessing, we need to vertically and horizontally translate one of the features and match again. The ranges of the vertical and horizontal translations are defined from -2 to 2 . The minimum D_o value obtained from the translated matchings is considered to be the final matching score.

4 EXPERIMENTAL RESULTS

4.1 Palmprint Database

We collected palmprint images from 193 individuals using our palmprint capture device. The subjects mainly consisted of volunteers from the students and staff at The Hong Kong Polytechnic University. In this dataset, 131 people are male, and the age distribution of the subjects is: younger than 30 years old is about 86%, older than 50 about 3%, with about 11% aged between 30 and 50. In addition, we collected the palmprint images on two separate occasions, at an interval of around two months. On each occasion, the subject was asked to provide about 10 images, each of the left palm and the right palm. We also gave some instructions to the subjects for using our capture device. Therefore, each person provided

around 40 images so that our database contained a total of 7,752 images from 386 different palms. In addition, we changed the light source and adjusted the focus of the CCD camera so that the images collected on the first and second occasions could be regarded as being captured by two different palmprint devices. The average time interval between the first and second occasions was 69 days. The maximum and minimum time intervals were 162 days and 4 days, respectively. Originally, the collected images were of two different sizes, 384×284 and 768×568. The larger image was resized to 384×284. Consequently, the size of all the test images used in the following experiments was 384×284 with 75dpi resolution. Fig. 8 shows three sets of preprocessed palmprint images that were captured at two different occasions. Their matching scores are shown in Table 1 (b). Note that the Hamming distances between two palmprint images from the same hand differ by, at most, 0.31. As a comparison, in the nine images that have similar principal lines from different people (see Fig. 4), the matching scores differ by, at least, 0.36, as shown in Table 1(a).

We also captured images under different lighting conditions (on the second occasion of image capture) to test the robustness of our algorithm. Typical samples are shown in Figs. 9 (a), (c), (e) for normal lighting, and in Figs. 9 (b), (d), (f) for special lighting. Their hamming distances are shown in Table 1(c). Although the lighting conditions shown in the second collection of images in Fig. 9 are quite different from the first collection, the proposed system can still easily recognize the same palm. This table gives an insight into the robustness of our system. The overall performance of our system is examined in the experiments described in the next sub-section.

4.2 Verification

To obtain the verification accuracy of our palmprint system, each of the palmprint images was matched with all of the palmprint images in the database. A matching is noted as a

correct matching if two palmprint images are from the same palm. The total number of matchings is 30,042,876. None of the hamming distances is zero. The failure to enroll rate is zero. The number of comparisons that have correct matching is 74,086 and the rest are incorrect matchings. The probability distributions for genuine and imposter are estimated by the correct and incorrect matchings, respectively, and are shown in Fig. 10(a). Fig. 10(b) depicts the corresponding Receiver Operating Characteristic (ROC) curve, which is a plot of genuine acceptance rate against false acceptance rate for all possible operating points. From Fig. 10(b), we can see that our system can operate at a 98% genuine acceptance rate and a 0.04% false acceptance rate, and the corresponding threshold is 0.3425. The system's equal error rate is 0.6%. This result is comparable with previous palmprint approaches and other hand-based biometric technologies including hand geometry and fingerprint verification [5-7,11,13-14,18-19].

4.3 Identification

Identification is a process of comparing one image against N images. In the following tests, we setup three registration databases for $N=50, 100$ and 200 , which are similar to the number of employees in small to medium sized companies. The first database contains 150 templates from 50 different palms, where each palmprints has three templates. Similarly for $N=100$ and 200 , the second and third registration databases have 300 and 600 templates, respectively. We also setup a testing database with 7,152 templates from 386 different palms. None of palmprint images in the testing database are contained in any of the registration databases. Each of the palmprint images in the testing database is matched with all of the palmprint images in the registration databases to generate incorrect and correct identification hamming distances. Since a registered palm has three templates in the registration databases, a palmprint image of a registered palm in the testing database is matched with its three templates in the registration databases to produce three correct hamming distances. We take

the minimum of these three distances as the correct identification hamming distances. Similarly, a palmprint image in the testing database is compared with all palmprint images in any registration database to produce $3N$ incorrect hamming distances if the testing palmprint does not have any registered images, or $3N-3$ incorrect hamming distances if the palmprint has three registered images. We take the minimum of these distances as the incorrect identification hamming distances. All the imposter identification distributions are generated using the 7,152 incorrect identification hamming distances. The genuine identification distributions are established using the 849, 1,702 and 3,414 correct hamming distances for $N = 50, 100$ and 200 , respectively. Figs. 11(a)-(c) illustrate the genuine and imposter distributions and the corresponding ROC curves are shown in Fig. 11(d). Comparing the imposter distributions of Figs. 11(a)-(c), when N increases, the imposter distribution moves to the left. This means that the average of the incorrect identification hamming distances is reducing. In the experiments, increasing N is equivalent to increasing the number of correct identification hamming distances to establish smoother genuine distributions. Fig. 11(d) shows that increasing N is equivalent to decreasing the accuracy of the system.

4.4 Speed

The system is implemented using Visual C++ 6.0 on an embedded Intel Pentium III processor (500MHz) PC. The execution time for the preprocessing, feature extraction and matching are 538ms, 84ms and 1.7ms, respectively. The total execution time is about 0.6 seconds, which is fast enough for real-time verification. For identification, if the database contains images for 100 persons, and each person registers three palmprint images, the total identification time is about 1.1 seconds. In fact, we have not yet optimized the program code so it is possible that the computation time could be reduced.

5 CONCLUSIONS

We have developed an on-line palmprint identification system for real-time personal identification by applying a novel CCD camera based palmprint device to capture the palmprint images. A preprocessing algorithm extracts a central area from a palmprint image for feature extraction. To represent a low-resolution palmprint image and match different palmprint images, we extend the use of 2-D Gabor phase coding to represent a palmprint image using its texture feature, and apply a normalized hamming distance for the matching measurement. Using this representation, the total size of a palmprint feature and its mask is reduced to 384 bytes. In our palmprint database of 7,752 palmprint images from 386 different palms, we can achieve high genuine (98%) and low false acceptance (0.04%) verification rates, and its equal error rate is 0.6%, which is comparable with all other palmprint recognition approaches. This result is also comparable with other hand-based biometrics, such as hand geometry and fingerprint verification [11,13-14]. For 1-to-100 identification, our system can operate at a 0.1% false acceptance rate and a reasonable 97% genuine acceptance rate. The execution time for the whole process, including preprocessing, feature extraction and final matching, is between 0.6 and 1.1 seconds on a Pentium III processor (500MHz).

In summary, we conclude that our palmprint identification system can achieve good performance in terms of speed and accuracy. For further improvement of the system, we will focus on three issues: 1) to reduce the size of the device for some special applications; 2) to combine the proposed palmprint coding scheme with other texture feature measurements such as texture energy for coarse-level classification to achieve higher performance, and 3) some noisy images with cuts and bruises on the hand have to be collected to test the system.

ACKNOWLEDGMENTS

The authors would like to thank Alex Feng, Brigitta Wan, Rex Fong and Chun-Sing Wong for their assistance in palmprint image collection. This research is partially supported by the UGC (CRC) fund from the Hong Kong SAR Government and the central fund from The Hong Kong Polytechnic University. The authors are also most grateful for the constructive advice and comments from the anonymous reviewers.

REFERENCES

- [1] A. Jain, R. Bolle and S. Pankanti (eds.), *Biometrics: Personal Identification in Networked Society*, Boston, Mass: Kluwer Academic Publishers, 1999.
- [2] D. Zhang, *Automated Biometrics – Technologies and Systems*, Boston: Kluwer Academic Publishers, 2000.
- [3] D. Zhang and W. Shu, “Two novel characteristics in palmprint verification: datum point invariance and line feature matching”, *Pattern Recognition*, vol. 32, no. 4, pp. 691-702, 1999.
- [4] N. Duta, A.K. Jain, and K.V. Mardia, “Matching of palmprint”, *Pattern Recognition Letters*, vol. 23, no. 4, pp. 477-485, 2001.
- [5] J. You, W. Li and D. Zhang, “Hierarchical palmprint identification via multiple feature extraction”, *Pattern Recognition*, vol. 35, no. 4, pp. 847-859, 2002.
- [6] W. Shu and D. Zhang, “Automated personal identification by palmprint”, *Optical Engineering*, vol. 37, no. 8, pp. 2659-2362, 1998.
- [7] W. Shi, G. Rong, Z. Bain and D. Zhang, “Automatic palmprint verification”, *International Journal of Image and Graphics*, vol. 1, no. 1, pp. 135-152, 2001.
- [8] <http://www.nectech.com/afis/download/PalmprintDtsht.q.pdf> - NEC automatic palmprint identification system.
- [9] P.S. Wu and M. Li, “Pyramid edge detection based on stack filter”, *Pattern Recognition Letter*, vol. 18, no. 4, pp. 239-248, 1997.
- [10] C.J. Liu and H. Wechsler, “A shape- and texture-based enhanced fisher classifier for face recognition”, *IEEE Transactions on Image Processing*, vol. 10, no. 4, pp. 598-608, 2001.
- [11] A.K. Jain, S. Prabhakar, L. Hong and S. Pankanti, “Filterbank-based fingerprint matching”, *IEEE Transactions on Image Processing*, vol. 9, no. 5, pp. 846-859, 2000.

- [12] J.G. Daugman, "High confidence visual recognition of persons by a test of statistical independence", *IEEE Transactions on Pattern Analysis and Machine Intelligence*, vol. 15, no. 11, pp. 1148-1161, 1993.
- [13] A.K. Jain, L. Hong and R. Bolle, "On-line fingerprint verification", *IEEE Transactions on Pattern Analysis and Machine Intelligence*, vol. 19, no 4, pp. 302-314, 1997.
- [14] R. Sanchez-Reillo, C. Sanchez-Avilla and A. Gonzalez-Marcos, "Biometric identification through hand geometry measurements", *IEEE Transactions on Pattern Analysis and Machine Intelligence*, vol. 22, no 18, pp.1168-1171, 2000.
- [15] R.P. Wildes, "Iris recognition: an emerging biometric technology", *Proceedings of the IEEE*, vol. 85, no 9, pp. 1348-1363, 1997.
- [16] D. Zhang (ed.), *Biometric Solutions for Authentication in an e-World*, Boston: Kluwer Academic Publishers, USA, 2002.
- [17] H.L. Lee and R.E. Gaensslen (eds.), *Advances in Fingerprint Technology*, 2nd ed. Boca Raton, FL: CRC press, 2001.
- [18] W. Li, D. Zhang and Z. Xu, "Palmprint identification by Fourier transform", *International Journal of Pattern Recognition and Artificial Intelligence*, vol. 16, no. 4, pp. 417-432, 2002.
- [19] C.C. Han, H.L. Cheng, K.C. Fan and C.L. Lin, "Personal authentication using palmprint features", *Pattern Recognition*, Special Issue: Biometrics, vol. 36, no 2, pp. 371-381, 2003.
- [20] <http://www.printrakinternational.com/omnitrak.htm> - Printrak automatic palmprint identification system.

FIGURES

- Fig. 1 Palmprint feature definitions with principal lines and wrinkles.
- Fig. 2 The design principle of the palmprint capture device.
- Fig. 3 The main steps of preprocessing. (a) Original image, (b) binary image, (c) boundary tracking, (d) building a coordinate system, (e) extracting the central part as a sub-image and (f) preprocessed result.
- Fig. 4 Three sets of the palmprint images with the similar principal lines
- Fig. 5 Typical preprocessed palmprint images without clear wrinkles.
- Fig. 6 (a) Incorrect placement of a palm and (b) the corresponding preprocessed image.
- Fig. 7 Feature features obtained by 2-D Gabor filtering. (a) Preprocessed images, (b) real parts of texture features, (c) imaginary parts of texture features and (d) the corresponding masks.
- Fig. 8 The palmprint images captured at the different time from the same person. (a), (c) and (e) first collected images; and (b), (d) and (f) second collected images.
- Fig. 9 Experimental results by the different lighting environments. (a), (c) and (e) normal condition and (b), (d) and (f) adjusted condition.
- Fig. 10 Verification test results. (a) Genuine and imposter distributions and (b) the receiver operator characteristic curve.
- Fig. 11 Identification test results. Genuine and imposter distributions for (a) $N = 50$, (b) $N = 100$, (c) $N = 200$ and (d) their receiver operating characteristic curves.

TABLE

- Table 1 The matching scores among the images in (a) Fig. 4, (b) Fig. 8 and (c) Fig. 9.

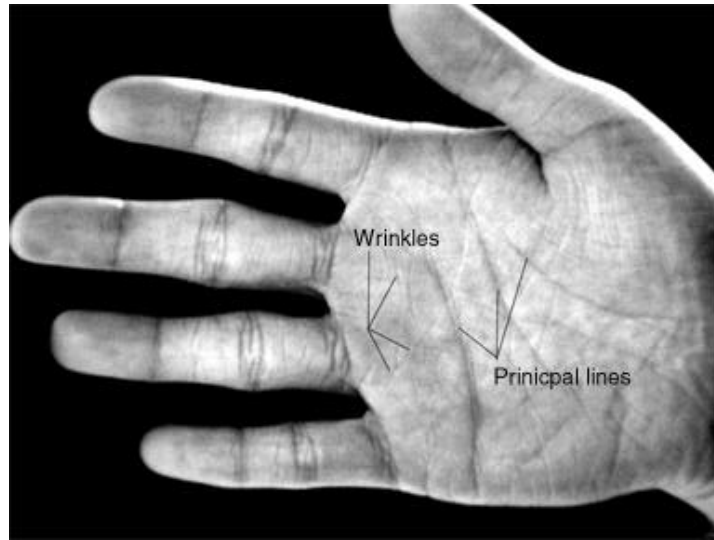


Fig. 1

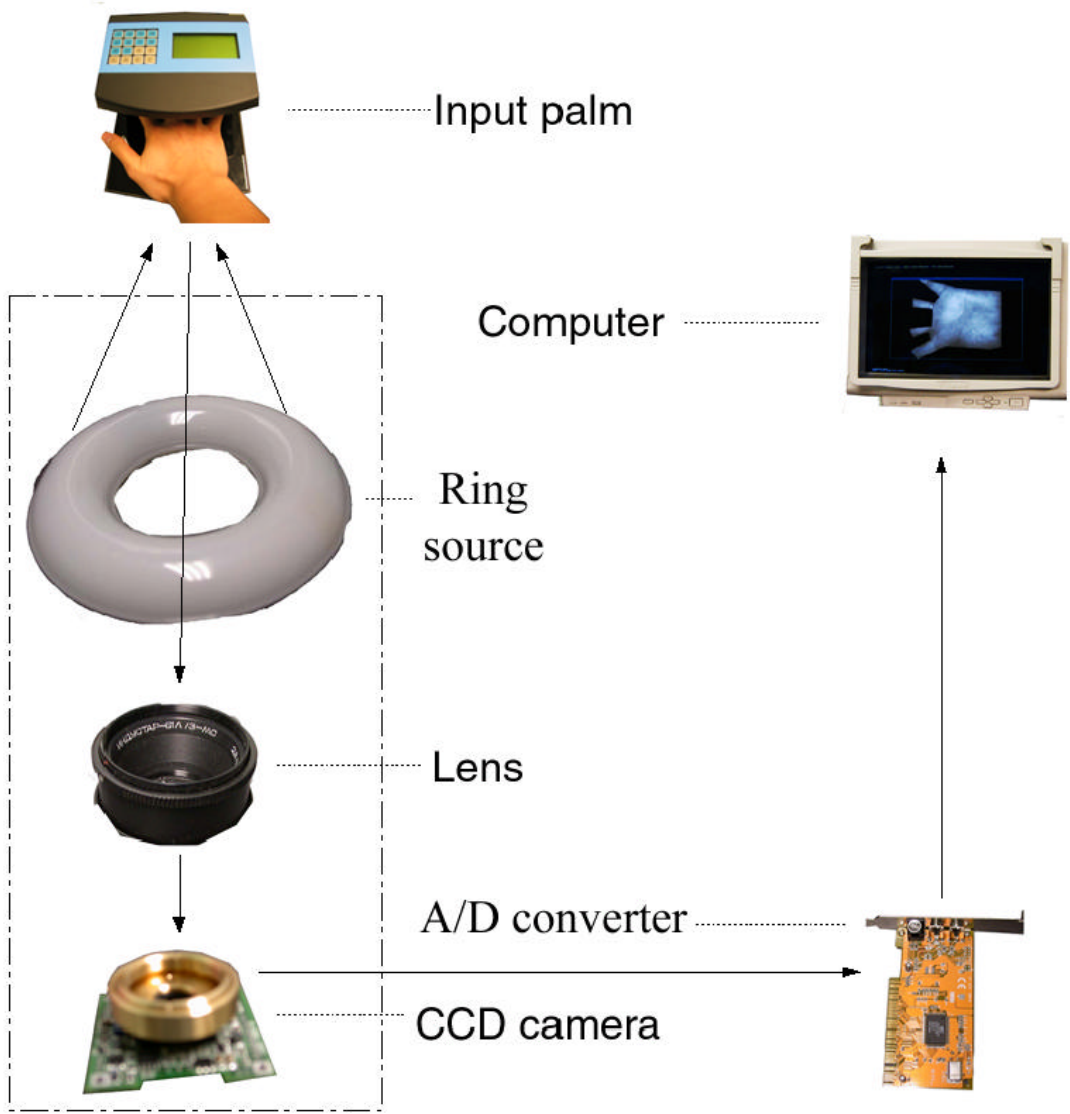


Fig. 2

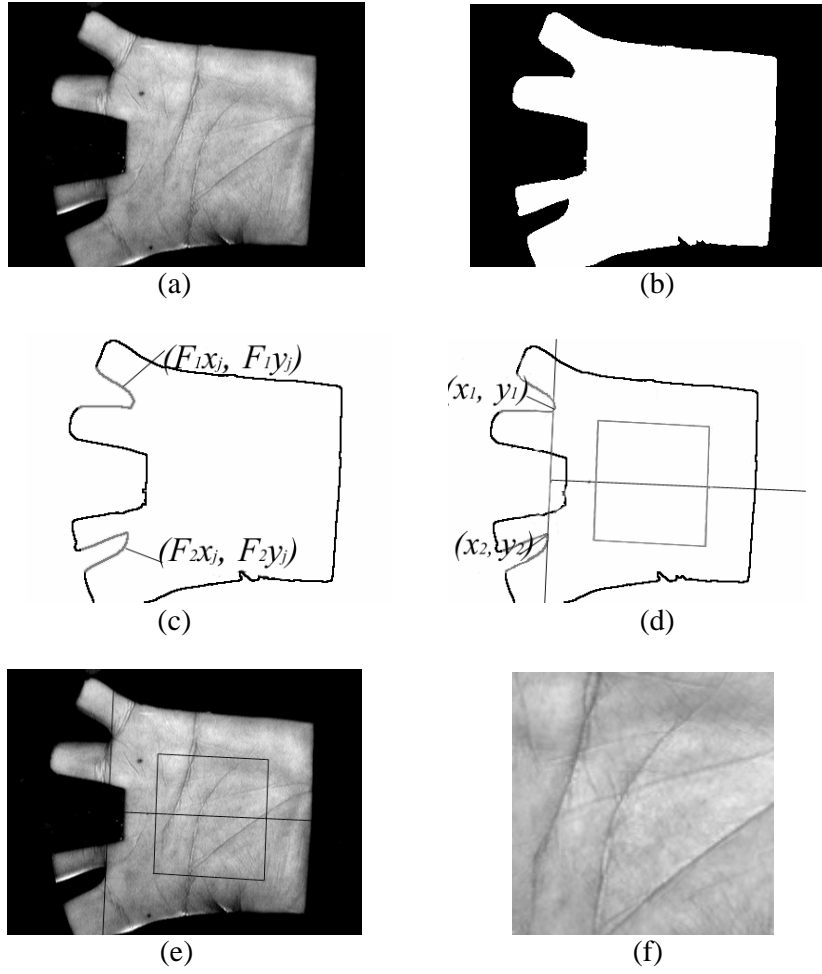


Fig. 3

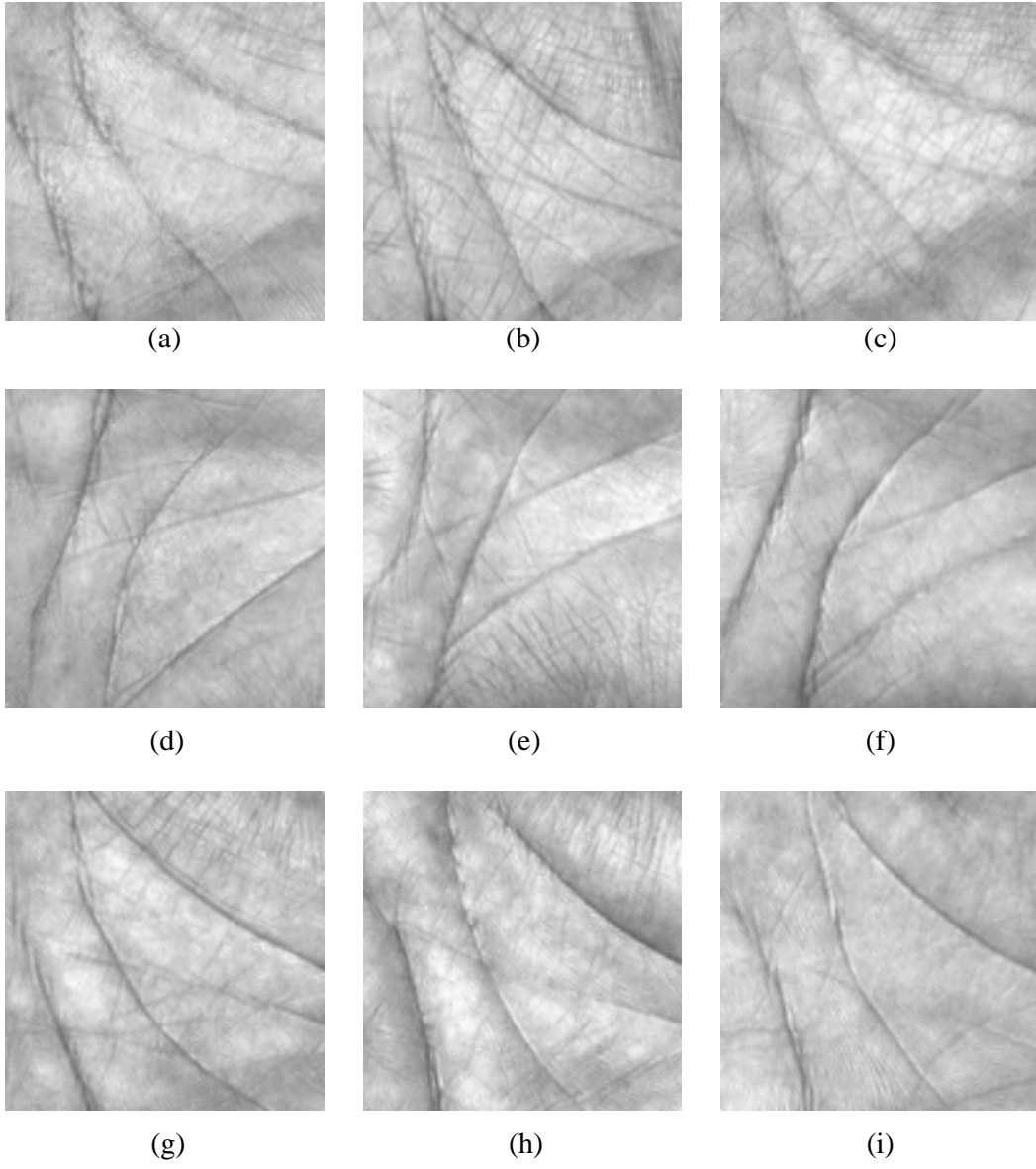


Fig. 4

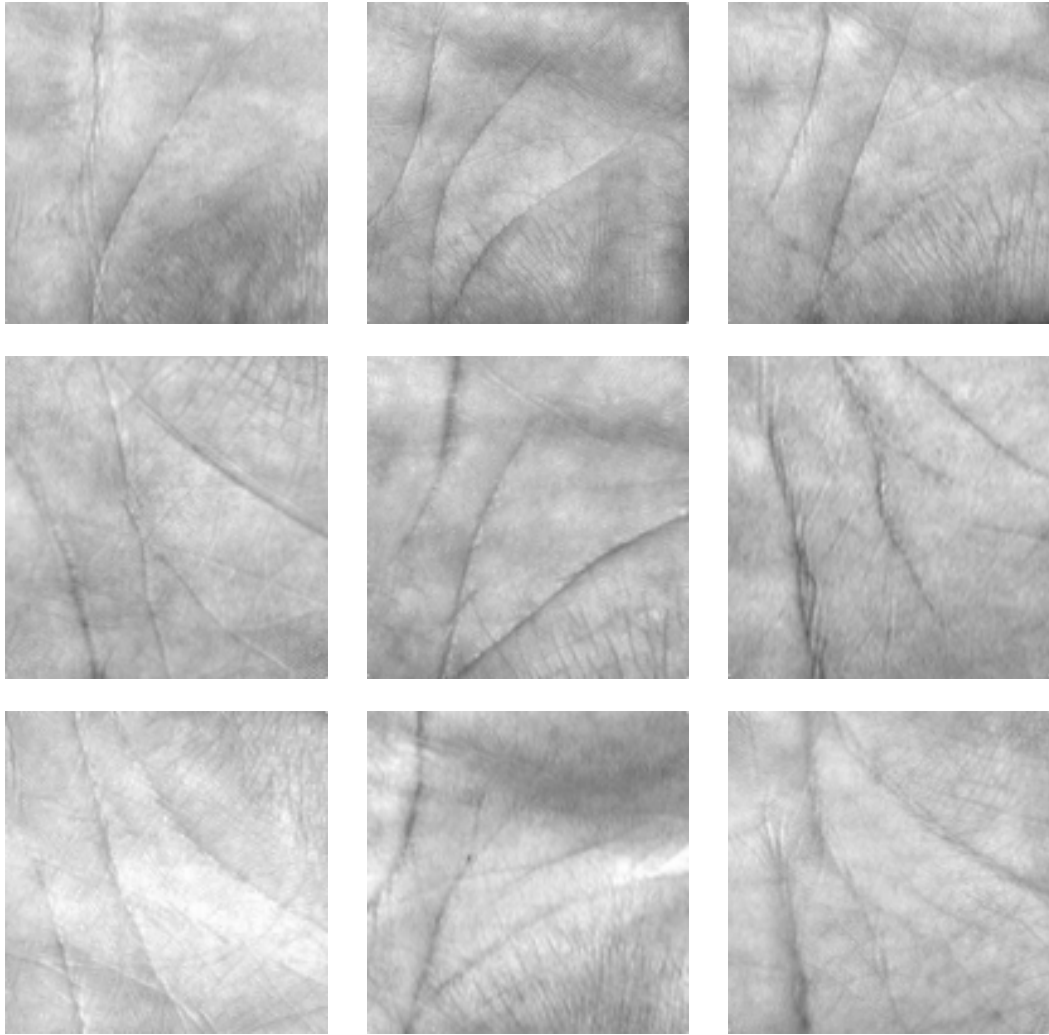
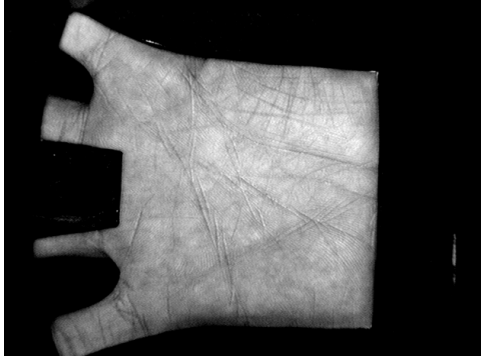
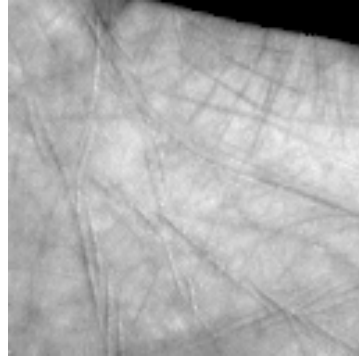


Fig. 5

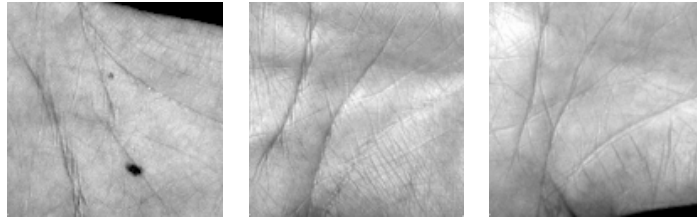


(a)

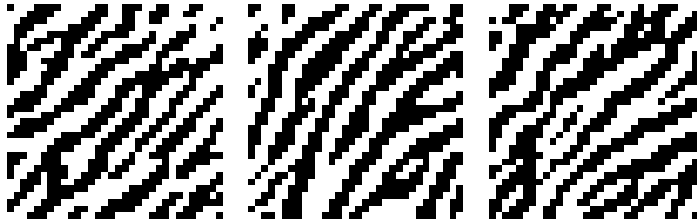


(b)

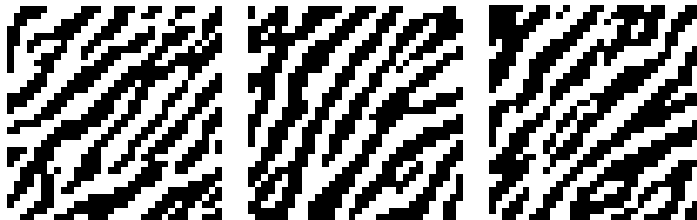
Fig. 6



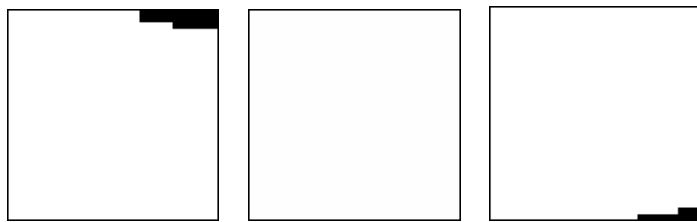
(a)



(b)

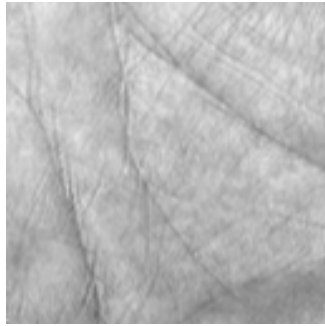


(c)

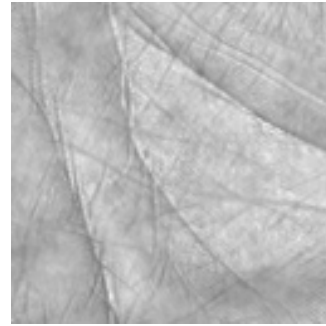


(d)

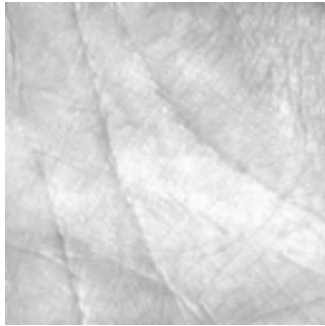
Fig. 7



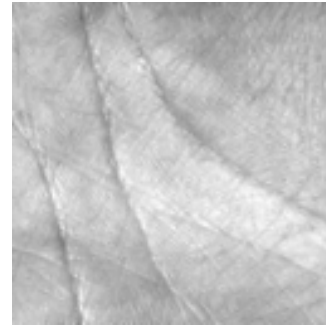
(a)



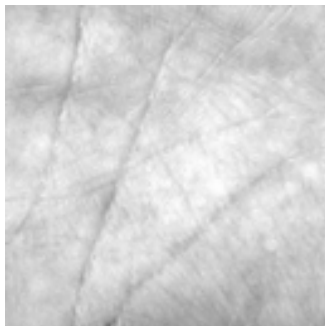
(b)



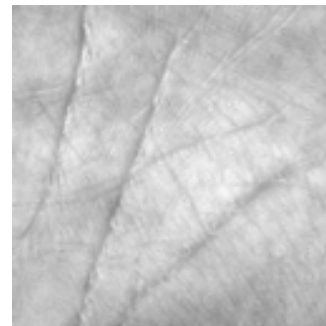
(c)



(d)

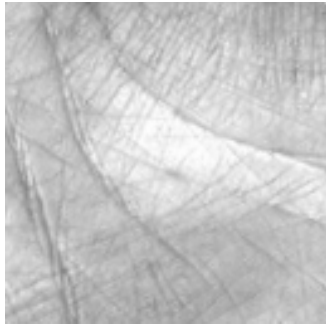


(e)

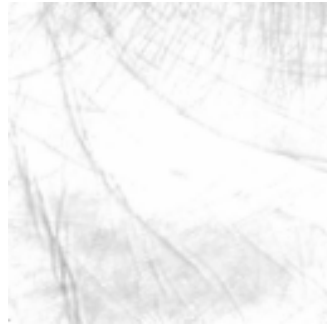


(f)

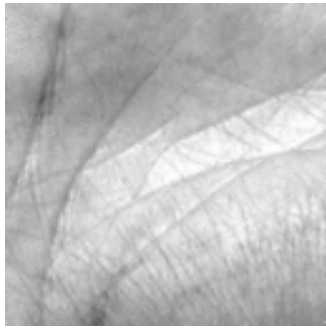
Fig. 8



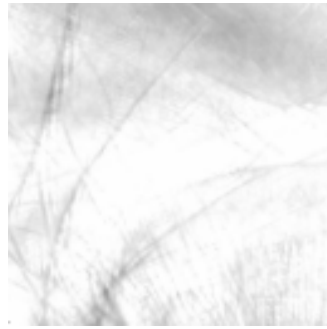
(a)



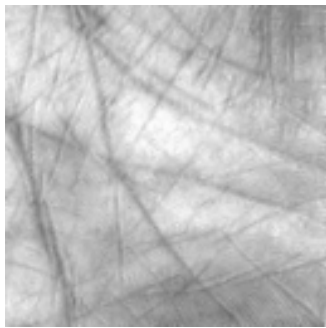
(b)



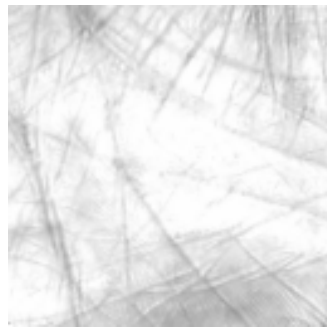
(c)



(d)

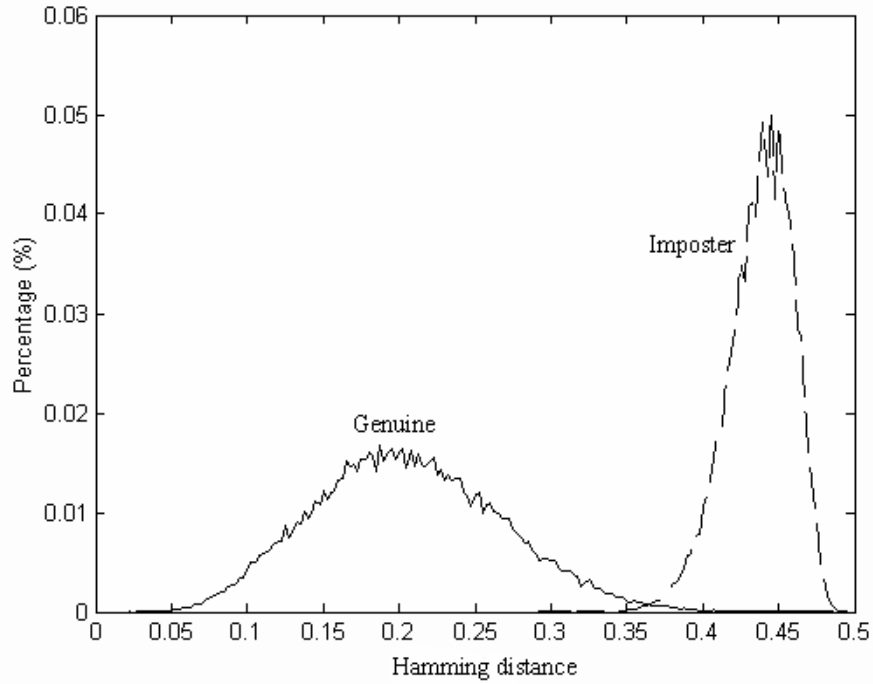


(e)

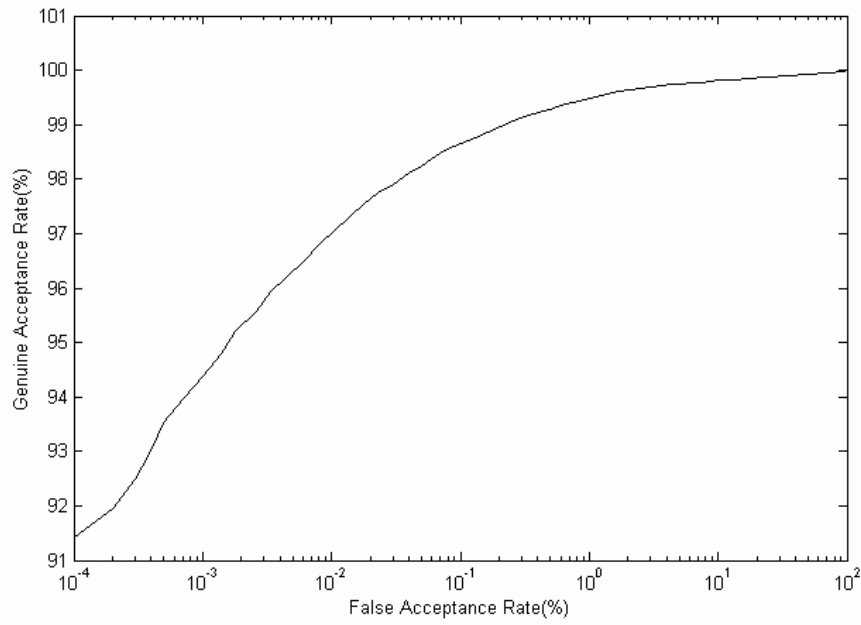


(f)

Fig. 9

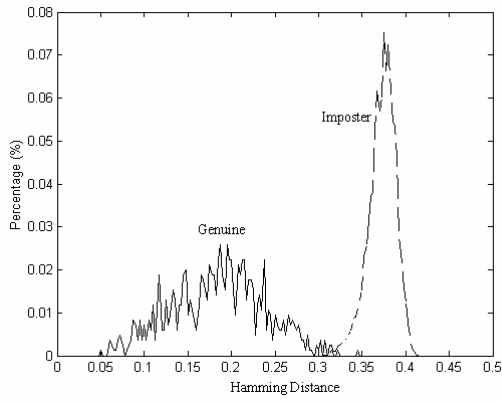


(a)

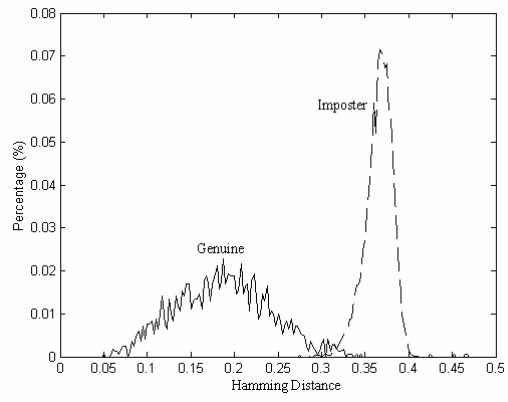


(b)

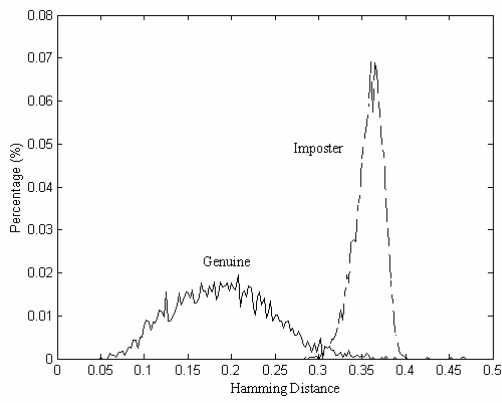
Fig. 10



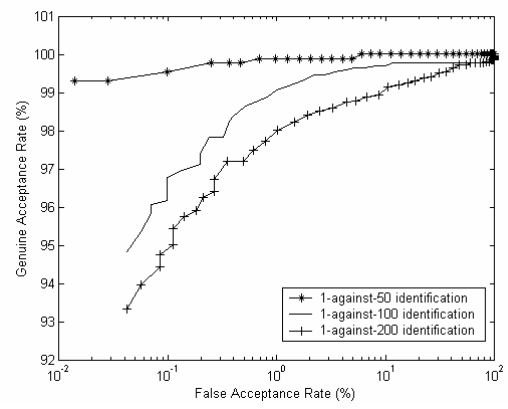
(a)



(b)



(c)



(d)

Fig. 11

Table 1

(a)

Figs	4(b)	4(c)	4(d)	4(e)	4(f)	4(g)	4(h)	4(i)
4(a)	0.44	0.47	0.43	0.43	0.47	0.46	0.44	0.44
4(b)		0.45	0.45	0.44	0.45	0.43	0.42	0.45
4(c)			0.39	0.48	0.39	0.39	0.44	0.48
4(d)				0.39	0.36	0.42	0.45	0.43
4(e)					0.42	0.41	0.45	0.42
4(f)						0.39	0.46	0.44
4(g)							0.45	0.45
4(h)								0.43

(b)

Figs	8(b)	8(c)	8(d)	8(e)	8(f)
8(a)	0.31	0.41	0.42	0.46	0.46
8(b)		0.43	0.42	0.46	0.46
8(c)			0.27	0.44	0.45
8(d)				0.42	0.42
8(e)					0.23

(c)

Figs	9(b)	9(c)	9(d)	9(e)	9(f)
9(a)	0.26	0.41	0.39	0.46	0.44
9(b)		0.42	0.4	0.45	0.45
9(c)			0.31	0.43	0.43
9(d)				0.43	0.46
9(e)					0.26